



168th Meeting of the Acoustical Society of America

Indianapolis, Indiana

27-31 October 2014

Noise: Paper 2aNSb1

Including source correlation and atmospheric turbulence in a ground reflection model for rocket noise

Kent L. Gee and Tracianne B. Neilsen

Department of Physics and Astronomy, Brigham Young University, Provo, UT; kentgee@byu.edu, tbn@byu.edu

Michael M. James

Blue Ridge Research and Consulting, LLC, Asheville, NC; michael.m.james@blueridgeresearch.com

Acoustic data collected in static rocket tests are typically influenced by ground reflections, but have been difficult to account for. First, the rocket plume is an extended radiator whose directionality results from source correlation. Second, partial coherence of the ground interaction due to atmospheric turbulence can play a significant role, especially for larger propagation distances. In this paper, a finite impedance-ground, single-source interference approach [G. A. Daigle, *J. Acoust. Soc. Am.* **65**, 45-49 (1979)] that incorporates both amplitude and phase variations due to turbulence is extended to distributions of correlated monopoles. The theory for obtaining the mean-square pressure from multiple correlated sources in the presence of atmospheric turbulence is described. The effects of source correlation, ground effective flow resistivity, and turbulence parameters are examined. Finally, the model predictions compared favorably against data from two horizontal firings of GEM-60 solid rocket motors – one involving snow-covered terrain – allowing effective removal of the ground reflection from far-field power spectral densities out to the maximum measurement distance of 1220 m. Close to the motor, more physically realistic corrected spectra are obtained by increasing the modeled fluctuating index of refraction by two orders of magnitude.



1. Background

In static rocket firings, such as the GEM-60 solid rocket motor test shown in Figure 1, the distributed, directional nature of the noise source, coupled with sound propagation over terrain and through the atmosphere, makes spectral predictions difficult. Because of the variable terrain, both in terms of impedance and topology, ground-based microphones are often impractical for static test environments and microphones are therefore elevated. However, ground reflection models based on a monopole source are unable to reasonably quantify multipath interference effects on radiated rocket noise. The radiation from different regions of the plume will be incident on the ground at different angles and their direct and reflected wave contributions will all superpose to yield the measured pressure at a microphone location. The present task examines the effect of a finite-impedance ground model that includes atmospheric turbulence on the radiation from arrays of correlated and uncorrelated sources. Military jet aircraft noise over a rigid ground has been previously modeled using line arrays of correlated and uncorrelated monopoles (Morgan *et al.*, 2012) meant to mimic the partially coherent nature of the jet noise source. A similar approach can be employed here to calculate the change in sound pressure level for correlated and uncorrelated source arrays due to a finite-impedance ground and atmospheric turbulence relative to free-field cases.

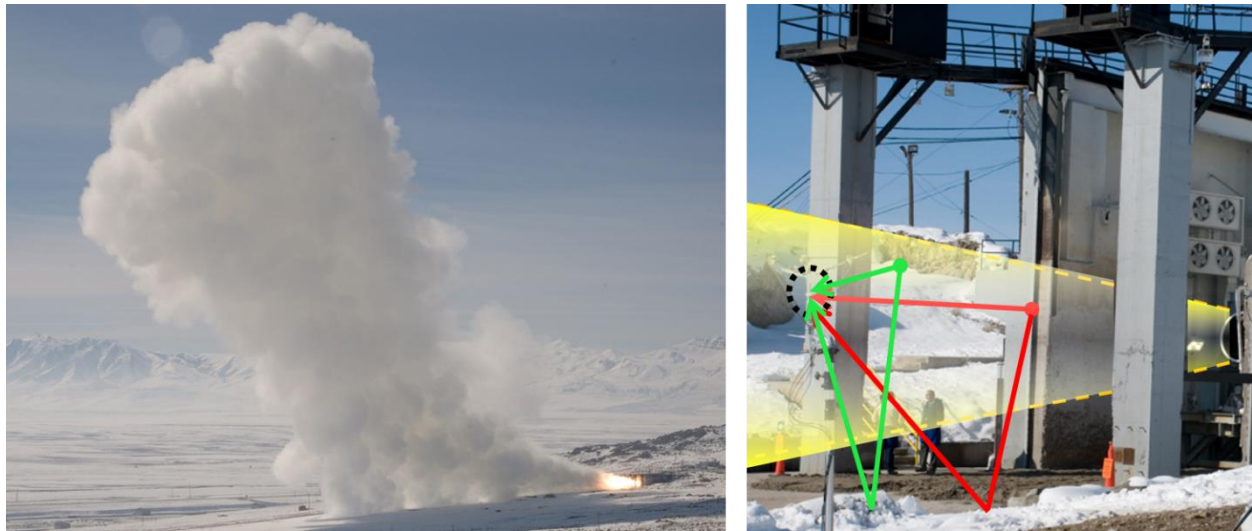


Figure 1. (Left) Distant view of a GEM-60 solid rocket motor firing. (Right) Schematic superimposed on a near-nozzle photograph showing how interference effects from multiple source locations might occur at the same microphone (dashed, black circle).

2. Theory

A. Foundational Models

To model the reflection of sound from a monopole with complex amplitude, $\mathbf{A} = Ae^{i\theta}$, off a finite-impedance ground at a receiver location, \mathcal{R} , (see Figure 2) we employ the extended-reacting ground approach by Embleton *et al.* (1983). In this model, the (complex) spherical reflection coefficient, $\mathbf{Q} = Qe^{i\gamma}$, is obtained by modeling the ground impedance using the “effective flow resistivity,” σ . (Delany, 1970) The direct and reflected path lengths are

shown as r_D , and r_R , respectively. This model, however, assumes a perfectly coherent interaction between the direct and reflected waves, a case that does not exist in practice because atmospheric turbulence that results in a partially coherent wave addition.

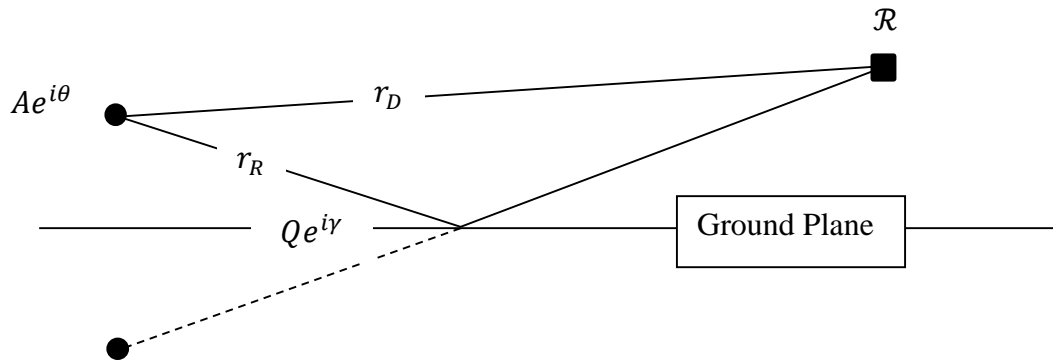


Figure 2. Source and image, with differing path lengths and complex spherical reflection coefficient, leading to multipath interference at receiver position, \mathcal{R} .

Although more complicated models exist for inclusion of turbulence in modeling of wave addition from ground reflections, Salomons *et al.* (2001) showed that an approach by Daigle (1978,1979,1983) is sufficiently accurate for most practical calculations. The model assumes a theory of homogenous, isotropic turbulence with Gaussian spatial correlation and both amplitude and phase fluctuations, and its solution assumes a large source-receiver separation distance. For a single source with unity amplitude, Daigle (1979) calculated the long-term average, mean-square pressure at the observer location, \mathcal{R} , for both amplitude and phase fluctuations, over a finite-impedance ground with impedance, $\mathbf{Q} = Qe^{i\gamma}$. We have recast his Eq. (10) in a different form, also allowing for a nonunity source amplitude, A , and can write the mean-square pressure as

$$\langle \overline{p^2} \rangle = A^2 \left[\frac{1 + \langle a^2 \rangle}{r_D^2} + Q^2 \frac{1 + \langle a^2 \rangle}{r_R^2} + \frac{2Q}{r_D r_R} \left[(1 + \langle a^2 \rangle \rho) \cos(\phi + \gamma) e^{-\sigma^2(1-\rho)} \right] \right]. \quad (1)$$

In Eq. (1), $\langle a^2 \rangle$ is the amplitude fluctuation, which is assumed to be the same for both the direct and reflected paths, $\phi = k(r_r - r_d)$, σ^2 is the variance of the turbulent phase fluctuation, and ρ is the amplitude and phase covariance function. (They are taken to be equal in the Daigle model). The parameters, $\langle a^2 \rangle$, σ^2 , and ρ can all be calculated for the geometry given two inputs, $\langle \mu^2 \rangle$ and L , which are the mean-square fluctuating index of refraction and the effective turbulence length scale, respectively. These can be measured or can represent adjustable empirical constants. Typical values for near-ground propagation are $\langle \mu^2 \rangle = 1 \times 10^{-5}$ and $L = 1.1$ m. Ranges of values for different ambient conditions are provided by Johnson *et al.* (1987). The ground impedance, \mathbf{Q} , is calculated according to Embleton *et al.*, (1983) which overcomes limitations described by Daigle in his paper. The first term in Eq. (1) represents the mean-square pressure, including turbulent fluctuations for the direct source (or path), whereas the second term represents the mean-square pressure for the image source or reflected path. The third term represents the interaction between the direct and image sources. If the turbulence is perfectly correlated over all space, $\rho \rightarrow 1$ and we have $[(1 + \langle a^2 \rangle) \cos(\phi + \gamma)]$ for the portion of the third term in the square brackets. Furthermore, if turbulent amplitude fluctuations are neglected and

$\langle a^2 \rangle \rightarrow 0$, the third term reduces to $2Q\cos(\phi + \gamma)/r_d r_r$, which is expected result for a perfectly coherent ground interaction.

B. Multi-source theoretical model

We now extend the model from a single spherical source to multiple sources, since any reasonable jet or rocket source model consists of an extended distribution. Recall that the previously developed jet noise model (Morgan, 2012) is comprised of line arrays of both uncorrelated and correlated monopoles. For the uncorrelated sources, the model can be implemented for each source, labeled m , and its image and the total mean-square pressure found by summing the mean-square pressure from each source. For M incoherent (denoted inc) sources, this summation is written as

$$\begin{aligned} \langle \overline{p^2} \rangle_{\text{inc}} &= \sum_{m=1}^M \langle \overline{p^2} \rangle_m \\ &= \sum_{m=1}^M A_m^2 \left[\frac{1 + \langle a^2 \rangle_m}{r_{D,m}^2} + Q_i^2 \frac{1 + \langle a^2 \rangle_m}{r_{R,m}^2} \right. \\ &\quad \left. + \frac{2Q_m}{r_{D,m} r_{R,m}} \left[(1 + \langle a^2 \rangle_m \rho_m) \cos(\phi_m + \gamma_m) e^{-\sigma_m^2 (1 - \rho_m)} \right] \right]. \end{aligned} \quad (2)$$

For correlated sources, a different approach is needed. We have returned to the roots of the Daigle method to consider the summation of two coherent sources of arbitrary amplitude and phase and their partially coherent images. The scenario is shown in Figure 3.

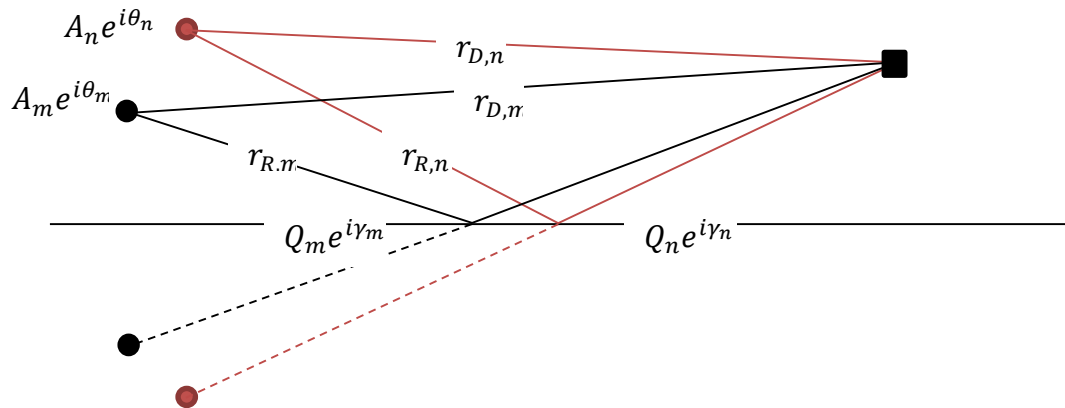


Figure 3. Geometry for the m th and n th sources.

In the Daigle model of multipath sound propagation through turbulence, amplitude and phase fluctuations are included by letting $A \rightarrow A(1 + a)$ and $kr \rightarrow kr + \delta$. The process of obtaining $\langle \overline{p^2} \rangle$ consists of writing the expressions for the four source terms in the complex pressure sum, finding its complex conjugate, multiplying the terms together, and then evaluating the long-term statistics of the turbulent fluctuations. The process involves multiple pages of algebra, but the answer is similar to that of the uncorrelated source, except it involves a total of 10 terms. The full expression may be written as

$$\begin{aligned}
\langle \overline{p^2} \rangle_{mn} = & \frac{A_m^2(1 + \langle a^2 \rangle)}{r_{D,m}^2} + Q_m^2 \frac{A_m^2(1 + \langle a^2 \rangle)}{r_{R,m}^2} + \frac{2A_m^2 Q_m}{r_{D,m} r_{R,m}} (1 + \langle a^2 \rangle \rho_1) \cos \phi_1 e^{-\sigma_1^2(1-\rho_1)} \\
& + \frac{A_n^2(1 + \langle a^2 \rangle)}{r_{D,n}^2} + Q_n^2 \frac{A_n^2(1 + \langle a^2 \rangle)}{r_{R,n}^2} + \frac{2A_n^2 Q_n}{r_{D,n} r_{R,n}} (1 + \langle a^2 \rangle \rho_2) \cos \phi_2 e^{-\sigma_2^2(1-\rho_2)} \\
& + \frac{2A_m A_n}{r_{D,m} r_{D,n}} (1 + \langle a^2 \rangle \rho_3) \cos \phi_3 e^{-\sigma_3^2(1-\rho_3)} \\
& + \frac{2A_m A_n Q_m}{r_{R,m} r_{D,n}} (1 + \langle a^2 \rangle \rho_4) \cos \phi_4 e^{-\sigma_4^2(1-\rho_4)} \\
& + \frac{2A_m A_n Q_n}{r_{D,m} r_{R,n}} (1 + \langle a^2 \rangle \rho_5) \cos \phi_5 e^{-\sigma_5^2(1-\rho_5)} \\
& + \frac{2A_m A_n Q_m Q_n}{r_{R,m} r_{R,n}} (1 + \langle a^2 \rangle \rho_6) \cos \phi_6 e^{-\sigma_6^2(1-\rho_6)}.
\end{aligned} \tag{3}$$

In Eq. (3), the variance and covariance terms, $\sigma_{1 \rightarrow 6}^2$ and $\rho_{1 \rightarrow 6}$, are evaluated for the paths involved in each of the six terms. (See Eqs. (12) and (17) in Daigle, 1979). The different angle terms, $\phi_{1 \rightarrow 6}$, are given as

$$\begin{aligned}
\phi_1 &= k(r_{D,m} - r_{R,m}) - \gamma_m \\
\phi_2 &= k(r_{D,n} - r_{R,n}) - \gamma_n \\
\phi_3 &= k(r_{D,m} - r_{D,n}) + (\theta_m - \theta_n) \\
\phi_4 &= k(r_{R,m} - r_{D,n}) + (\theta_m - \theta_n) + \gamma_m \\
\phi_5 &= k(r_{D,m} - r_{R,n}) + (\theta_m - \theta_n) - \gamma_n \\
\phi_6 &= k(r_{R,m} - r_{R,n}) + (\theta_m - \theta_n) + (\gamma_m - \gamma_n).
\end{aligned}$$

The first two lines in Eq. (3) represent the *independent* squared pressure (with the mean-square effects of turbulence) of the *m*th and *n*th sources and their images in the absence of intersource coupling, similar to Eq. (2). The remaining four lines represent the partially coherent coupling between the *m*th and *n*th source/image combinations.

Note again that that this represents the summation of just two sources. Extension of this partially coherent addition for *M* sources means that that we represent the overall squared pressure as the sum of the incoherent contributions in Eq. (2) and the cross-coupling terms (the last four lines) in Eq. (3). If we define these cross coupling terms as

$$\begin{aligned}
\langle \overline{p^2} \rangle_{\text{cross}} &= \frac{2A_m A_n}{r_{D,m} r_{D,n}} (1 + \langle a^2 \rangle \rho_3) \cos \phi_3 e^{-\sigma_3^2(1-\rho_3)} \\
&+ \frac{2A_m A_n Q_m}{r_{R,m} r_{D,n}} (1 + \langle a^2 \rangle \rho_4) \cos \phi_4 e^{-\sigma_4^2(1-\rho_4)} \\
&+ \frac{2A_m A_n Q_n}{r_{D,m} r_{R,n}} (1 + \langle a^2 \rangle \rho_5) \cos \phi_5 e^{-\sigma_5^2(1-\rho_5)} \\
&+ \frac{2A_m A_n Q_m Q_n}{r_{R,m} r_{R,n}} (1 + \langle a^2 \rangle \rho_6) \cos \phi_6 e^{-\sigma_6^2(1-\rho_6)},
\end{aligned} \tag{4}$$

we can express the total summation between the coherent sources as

$$\langle \overline{p^2} \rangle_{\text{coh}} = \langle \overline{p^2} \rangle_{\text{inc}} + \sum_{m=1}^{M-1} \sum_{n=m+1}^M \langle \overline{p^2} \rangle_{\text{cross}} \quad (5)$$

3. Application to Rocket Noise

A. Solid Rocket Motor Data

The primary goal of applying this model to rocket noise is to examine results of the multisource ground reflection model applied to solid rocket motor firings with vastly different ground cover, i.e., relatively hard ground and snow. Data were collected during GEM-60 static rocket motor firings (1.09 m exit diameter, 875 kN thrust) in February 2009 (see Figure 1 and left of Figure 4) and September 2012 (right of Figure 4) at the T-6 ATK test facility near Promontory, Utah. For the February firing, the ground was covered with approximately 15-30 cm (6 -12 in) of snow, depending on location. The February 2009 test has been described in previous publications by Gee *et al.* (2009) and Muhlestein *et al.* (2013). The 2009 test included type-1 GRAS 40BD pressure microphones located at 76, 152, and 305 m located along 50° and 60° relative to the plume exhaust centerline and a reference point 8.5 m downstream of the nozzle. Microphones were placed at heights of 1.5-2 m, whereas the motor centerline was located at a height of 3.2 m. For the 2012 test, microphones to be analyzed here were located at 19, 109 and 218 m along a 60° radial relative to reference position 18.6 m downstream. (The greater downstream origin location was based on an improved understanding of the dominant noise source location after the 2009 measurements, but for the purpose of this analysis, all distances are referenced relative to their respective origins.) In the 2012 test, the GRAS pressure microphones were located at approximately the 3.2 m nozzle height. For both tests, measurements were also made at the test observation location, which was approximately 1220 m away on a sloping cliff edge 45 m high and along the 60° radial (see Figure 4). The power spectral densities (PSDs) along the two radials and at the 1220 m measurement location are displayed in Figure 5 - Figure 7. The characteristic jet or rocket haystack spectral shape is evident in all measurements, along with evidence of multipath interference in some cases.



Figure 4. Photographs taken from the test observation location during the February 2009 (left) and September 2012 (right) GEM-60 firings.

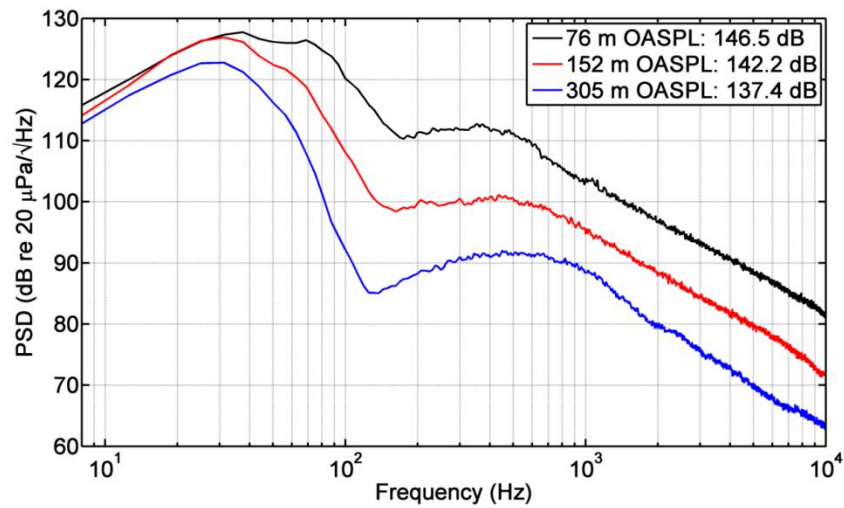


Figure 5. Power spectral densities along the 50° radial from the 2009 GEM-60 firing.

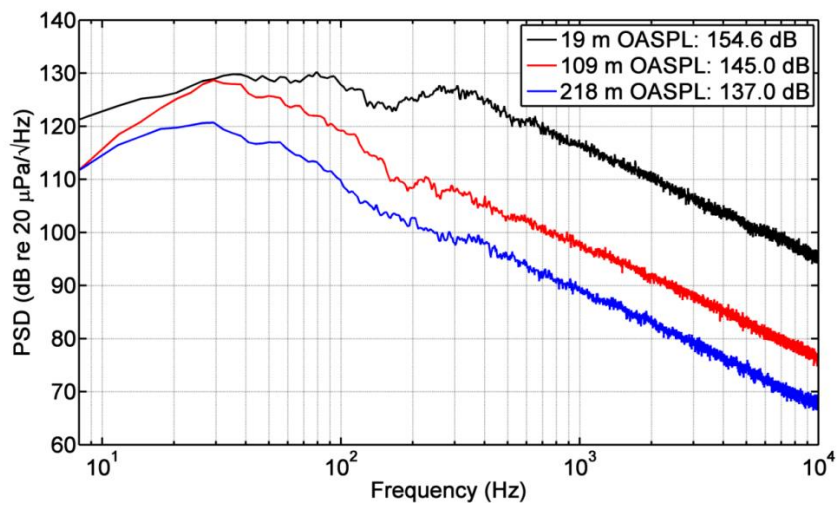


Figure 6. Power spectral densities along the 60° radial from the 2012 GEM-60 firing.

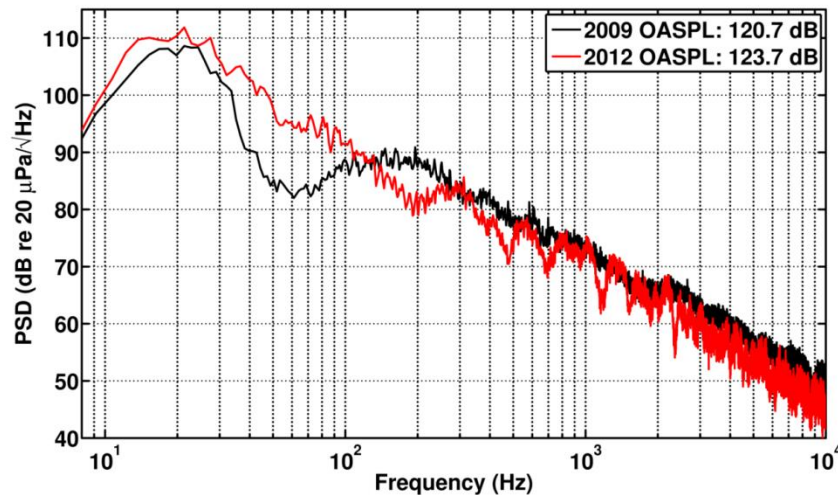


Figure 7. Power spectral densities at the 1220 m measurement location along the 60° radial from both motor firings.

B. Source Distribution

Although a simple source-based model exists for rocket noise in the form of the prediction methods outlined in NASA SP-7072 (Eldred, 1971), there is not an equivalent source model for rocket noise incorporating realistic correlated source distributions. However, because only the *relative* sound pressure level, Δ SPL, due to the ground is of interest in this paper, a frequency-independent Rayleigh amplitude and slowly varying phase distributions were selected for use. Other sources were tried, e.g., a 25-m line source with two periods of phase variation, but results obtained from calculations as a function of range and height to the side of the distribution maximum in Figure 8 are very similar to those shown subsequently. A more rocket-like source distribution remains subject of future investigations, but the initial results suggest the validity of the overall reasoning here.

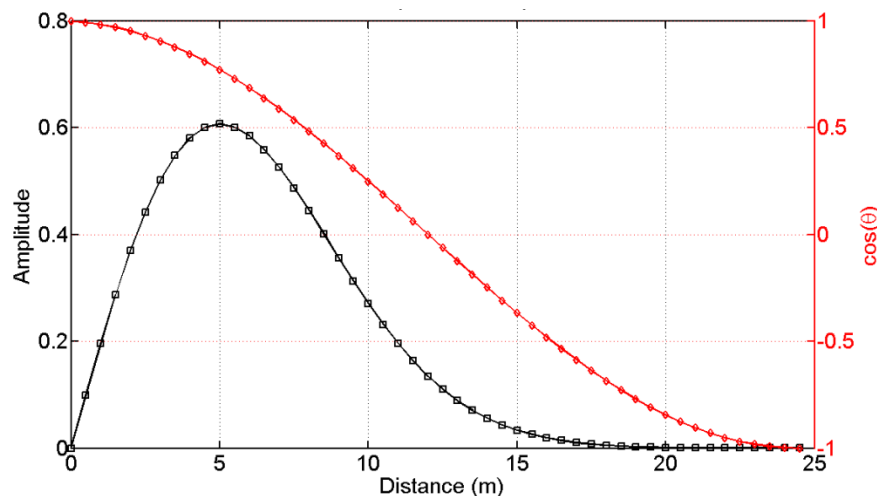


Figure 8. Assumed frequency-independent amplitude and phase source distributions.

C. Exercising of Source Model

The source model has been used to investigate the effect of ground impedance and atmospheric parameters on the relative sound pressure level, ΔSPL , for both the 2009 and 2012 measurement geometries. The ground impedance has been calculated for the 2009 test by assuming $\sigma = 30$ cgs rayls and for the 2012 test by assuming $\sigma = 3000$ cgs rayls. These fall within the range of parameters provided by Embleton *et al.* (1938) for snow (10 – 50 cgs rayls), and between hard-packed sandy silt (800 – 2500 cgs rayls) and exposed, rain-packed earth (4000 – 8000 cgs rayls). Values for $\langle\mu^2\rangle$ and L , (the mean-square fluctuating index of refraction and the effective turbulence length scale, respectively) were selected based on the work by Johnson *et al.* (1987). On both days, the conditions were relatively sunny and the winds were light (<2 m/s) to moderate (2-4 m/s). Consequently, $\langle\mu^2\rangle = 10^{-5}$ was used as the baseline fluctuating index of refraction and L was increased with height beginning from a value of $L = 1.1$ m at a microphone height of 1.5 m.

Figure 9 shows calculations for ΔSPL at the 305 m location for the 2009 test using the assumed parameters provided in the caption. Four cases are shown: an incoherent (uncorrelated) and a coherent (correlated) Rayleigh distribution from Figure 8, with and without atmospheric turbulence. Note that because the range is much greater than the source extent, ΔSPL for coherent and incoherent sources without turbulence collapse nearly exactly and are also essentially identical to that of a monopole. A 6 dB boost in level at low frequencies caused by effectively superposing the source and image is followed by a broad interference null resulting from the soft, snow-covered ground. An additional high-frequency interference null is seen at approximately 10 kHz for the non-turbulent cases. It is the partial coherence between the source/image paths and the sources (for the coherent case) when turbulence is present that completely removes the presence of this null. Again, given that the distance from source to receiver is much greater than the source dimensions, the incoherent source distribution with turbulence is essentially identical to that of a monopole: The 6 dB boost at low frequencies due to coherent pressure addition gives way to a 3 dB increase at high frequencies because the direct and reflected path signals are essentially incoherent. The partially coherent interaction at mid frequencies effectively reduces the depth of the interference null. In the case of the correlated Rayleigh distribution, it is the partially coherent interaction between all the source/image combinations that reduces the depth of the interference null from that of the incoherent source case.

Figure 10 shows the four source/turbulence combinations for the 2012 test at the 218 m location for the estimated conditions. The significantly harder ground pushes the initial interference null to much higher frequencies and then for the non-turbulent calculations, they continue at nearly regular intervals. Again, the turbulence reduces the number of interference nulls to one, and in the case of the correlated sources, eliminates it almost entirely. To investigate the effects of independently changing parameters, two additional cases are shown in Figure 11 and Figure 12. In Figure 11, the impact of an essentially infinite ground impedance is tested. Without turbulence, the nulls increase in frequency and in depth, but with turbulence, the depth of the turbulent interference nulls is reduced. In Figure 12, the turbulent fluctuating index of refraction is increased by an order of magnitude relative to Figure 10, again reducing the depth of both of the turbulence-included ΔSPL curves. However, the change in ΔSPL for the coherent-source case is less significant than the incoherent-source case. These examples help to illustrate some of the changes expected in the model for different parameter choices for the same geometry.

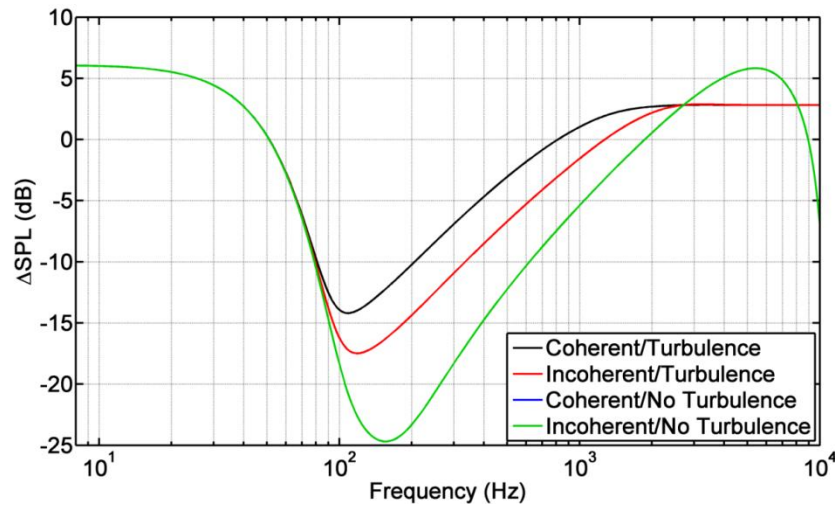


Figure 9. Relative sound pressure level for 2009 GEM-60 test at 305 m, with a 1.5 m microphone height, $\sigma_{eff} = 30$ cgs rays, $L = 1.1$ m, and $\langle \mu^2 \rangle = 1 \times 10^{-5}$.

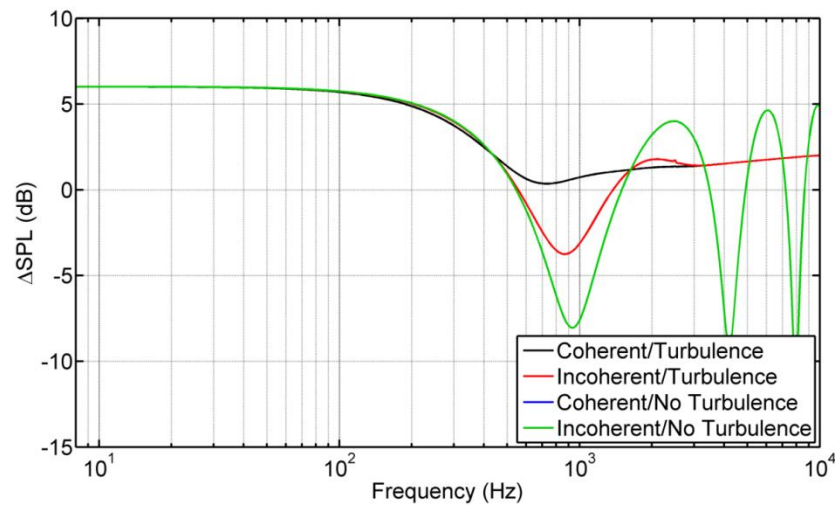


Figure 10. Relative sound pressure level for 2012 test at 218 m, with a 3.2 m microphone height, $\sigma_{eff} = 3000$ cgs rays, $L = 2.5$ m, and $\langle \mu^2 \rangle = 1 \times 10^{-5}$.

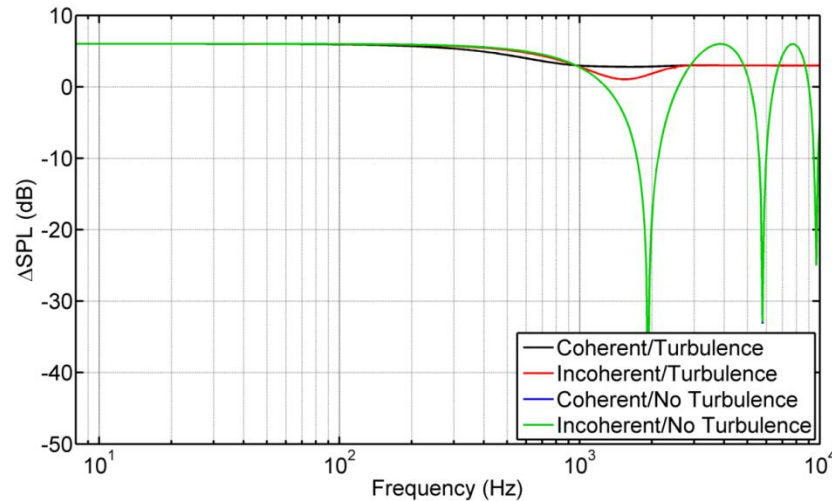


Figure 11. Relative sound pressure level for 2012 test at 218 m, with a 3.2 m microphone height, $\sigma_{eff} = 3 \times 10^7$ cgs rays, $L = 2.5$ m, and $\langle \mu^2 \rangle = 1 \times 10^{-5}$.

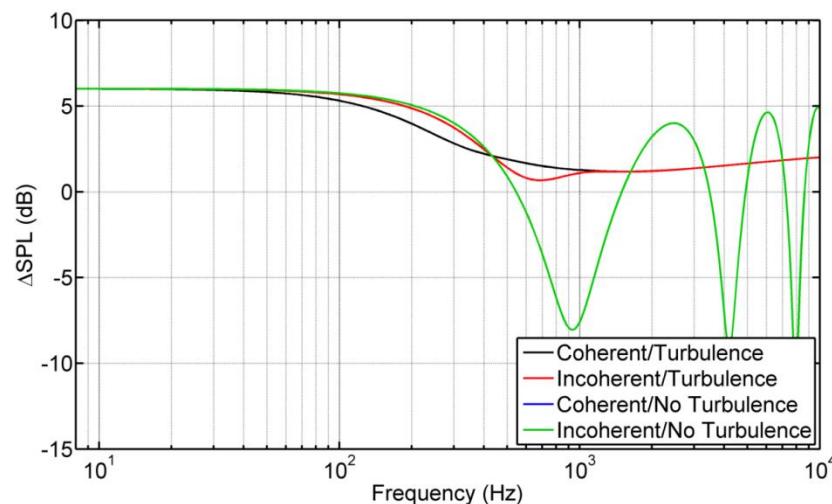


Figure 12. Relative sound pressure level for 2012 test at 218 m, with a 3.2 m microphone height, $\sigma_{eff} = 3000$ cgs rays, $L = 2.5$, and $\langle \mu^2 \rangle = 1 \times 10^{-4}$.

D. Ground Reflection Correction of Measured Rocket Spectra

The ground and turbulence parameters that produced the “Coherent/Turbulence” curves in Figure 9 and Figure 10 were used to create corrections for the 2009 and 2012 test PSDs. These results are shown in Figure 13 – Figure 15. Subtraction of the calculated Δ SPL curves from the measured 2009 spectra in Figure 5 removes much or all of the interference null at all three locations and creates more realistic power-law based spectral shapes in Figure 13 that are characteristic of jet and rocket noise, e.g. (Eldred, 1971), (Tam, 1995), (Neilsen, 2013). The corrected PSD at 76 m appears to create some ringing in the mid-frequency region that was not originally present in the data, but overall, the new model summarized by Eq. (5) appears to offer improvement in spectral characterizations over the raw PSD.

For the 2012 test, correction of the 19 m PSD (see Figure 6) is postponed until the next section. For the 2012 data at 109 and 218 m, there was little evidence of ground interference effects in Figure 6. Consequently, the Δ SPL corrections must mimic this behavior, as was shown in Figure 10. The corrected PSDs for these two distances are shown, along with the original PSDs, in Figure 14. The correction serves mostly to reduce the amount of low-frequency energy while leaving the spectral levels above 400 Hz relatively untouched. This results in an altered spectral shape, particularly at 109 m. The physicality of either result cannot be verified at this stage, but it is encouraging that both the measurement and the coherent-source, turbulent ground reflection model indicate the absence of interference nulls.

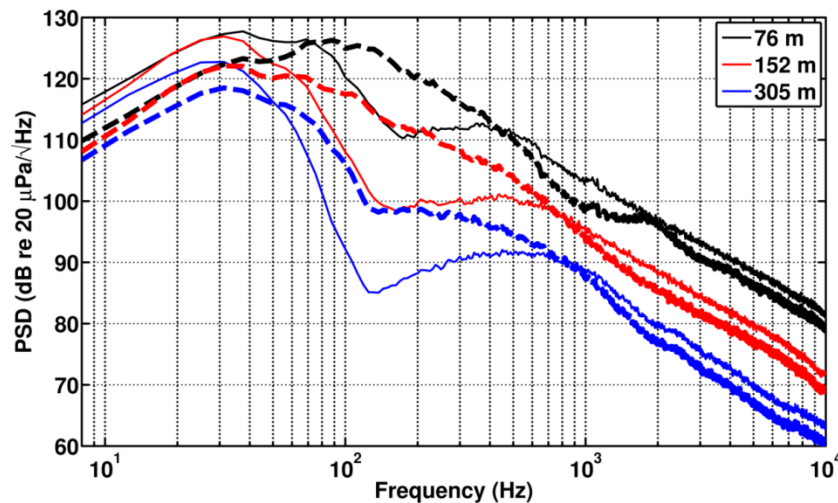


Figure 13. Measured (see Figure 5) and ground-corrected spectra (dashed lines) from the 2009 GEM-60 firing.

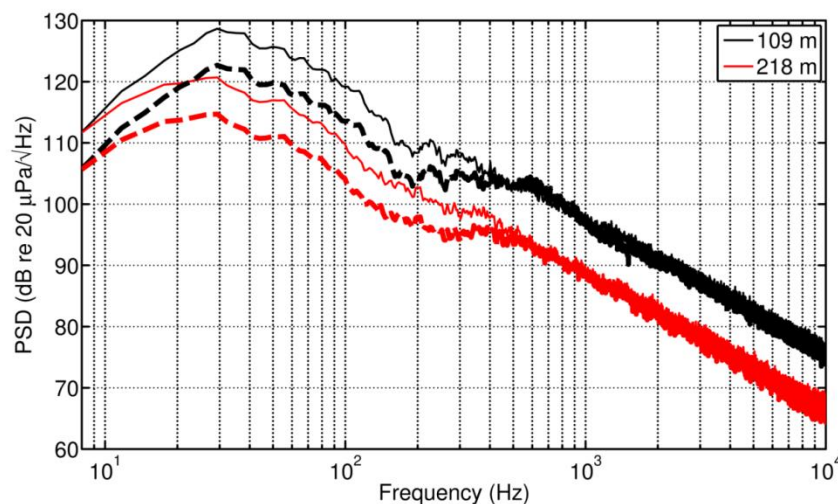


Figure 14. Measured (see Figure 6) and ground-corrected spectra (dashed lines) from the 2012 GEM-60 firing at 109 and 218 m.

At 1220 m, the two spectra shown previously in Figure 7 have now been corrected using the same turbulence parameters, $L = 7.0$ m and $\langle \mu^2 \rangle = 1 \times 10^{-5}$, but with the respective flow resistivities for the soft and hard ground. Although the Johnson *et al.* results suggest that a

greater turbulence length scale be used for a microphone height of 45 m, the somewhat arbitrary choice of $L = 7.0$ m is based on the fact that the terrain slopes upwards toward cliff near the measurement point and therefore the microphone is not actually located that far from the ground. Values for $L = 5.0$ to $L = 10.0$ gave similar results for ΔSPL , so the choice of $L = 7.0$ seems relatively robust. The measured PSDs in Figure 15 showed the greatest difference between the two spectra below 100 Hz. By correcting them using their respective ground impedances and the same turbulence parameters, the two spectra now nearly overlay each other below 100 Hz where the spectral differences were the largest. The fact that two spectra measured more than a kilometer from two different firing made at two very different times of year overlay each other with such consistency is remarkable in and of itself!

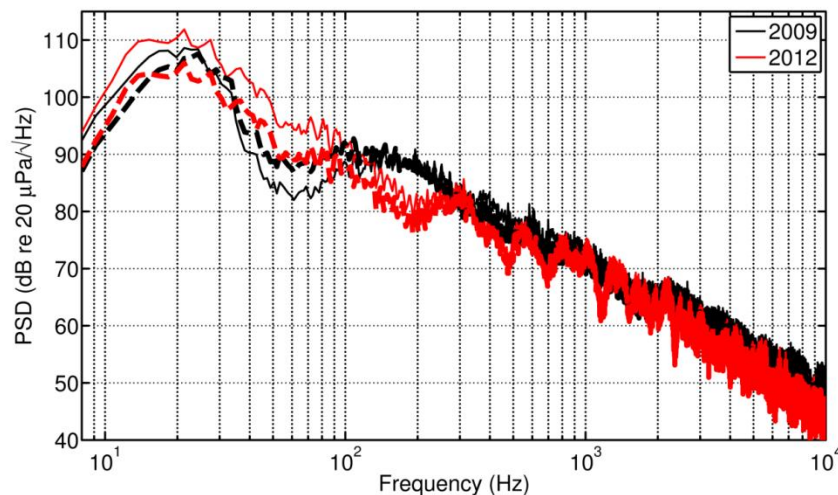


Figure 15. Measured (see Figure 7) and ground-corrected spectra (dashed lines) from the 2009 and 2012 GEM-60 firing at 1220 m. In both cases, $L = 7.0$ m and $\langle\mu^2\rangle = 1 \times 10^{-5}$ was used.

E. Accounting for Near-Source Atmospheric Turbulence

We have held off discussing the 19 m PSD from the 2012 test until this point because attempts to apply the coherent-source ground reflection model in Eq. (5) with the same turbulence parameters as used at 109 and 218 m reveals that the measured interference null is far shallower than what the model would predict; i.e., the propagation paths are too short to account for such a shallow interference null. This shallow interference null could be caused by the rocket being a volume rather than a line source and this concept needs to be investigated. On the other hand, the rocket plume entrains air and also produces nonacoustic temperature variations in the near field (Giraud, 2010). Given these physical realities, it may be possible to model the shallower measured interference null using an increased fluctuating index of refraction and or turbulence length scale, while allowing at the outset that $\langle\mu^2\rangle$ and L become empirical constants in that that measurements of these parameters near a rocket do not exist. In this light, only variations in $\langle\mu^2\rangle$ are considered at this time. Figure 16 - Figure 19 contain the measured and corrected PSDs for $\langle\mu^2\rangle$ ranging four orders of magnitude – between $\langle\mu^2\rangle = 1 \times 10^{-5}$ to $\langle\mu^2\rangle = 1 \times 10^{-2}$. Figure 16 and Figure 17 show that $\langle\mu^2\rangle$ is too low in that subtraction of the ΔSPL from the measure PSD results in sharp spectral peaks. On the other hand, Figure 19 shows only a smooth reduction in spectral levels, meaning that no interference null was predicted (like at 109

and 218 m). It is the result in Figure 18 that is intriguing – the interference null has been replaced by a smooth power-law spectrum whose maximum actually falls within the prior null region. There is no means of determining whether this PSD is the correct free-field PSD, but the result is plausible and suggests that the fluctuating index of refraction needs to be increased near the rocket plume.

This hypothesis suggests it worthwhile to revisit the 76 – 305 m PSDs from the data; the 76 m data, in particular, suffered from a mid-frequency ringing that was perhaps indicative of $\langle \mu^2 \rangle$ being too low. To further test the idea that near-plume propagation is affected by greater turbulence, the Δ SPL prediction for 76 m has been modeled with an increase in $\langle \mu^2 \rangle$ by one order of magnitude to $\langle \mu^2 \rangle = 1 \times 10^{-4}$. For 152 m, the turbulence parameter has been increased to $\langle \mu^2 \rangle = 5 \times 10^{-5}$. These choices are arbitrary but are at least bounded by the 2012 19 m results and the “far-field” value of $\langle \mu^2 \rangle = 1 \times 10^{-5}$. The change in the 76 and 152 m PSD corrections are noticeable and result in an improved power-law spectral shape. This suggests that this near-ground propagation can, in fact, be modeled using a correlated source distribution and turbulence parameters that are significantly larger than those ordinarily encountered in outdoor propagation scenarios.

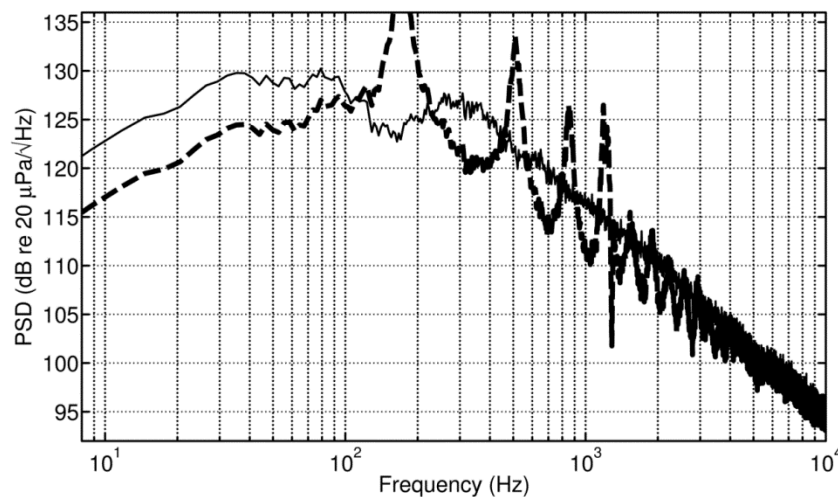


Figure 16. Measured and corrected PSDs using a 3.2 m microphone height, $\sigma_{eff} = 3000$ cgs rayls, $L = 2.5$ m, and $\langle \mu^2 \rangle = 1 \times 10^{-5}$.

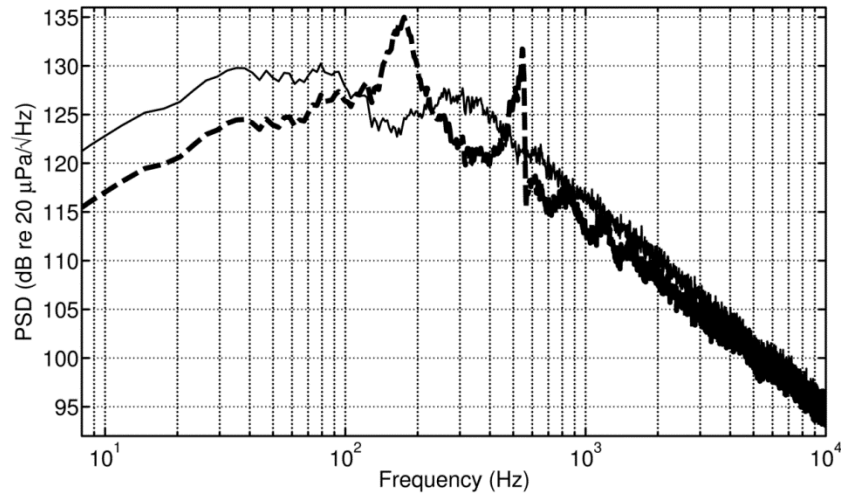


Figure 17. Measured and corrected PSDs using a 3.2 m microphone height, $\sigma_{eff} = 3000$ cgs rayls, $L = 2.5$ m, and $\langle \mu^2 \rangle = 1 \times 10^{-4}$.

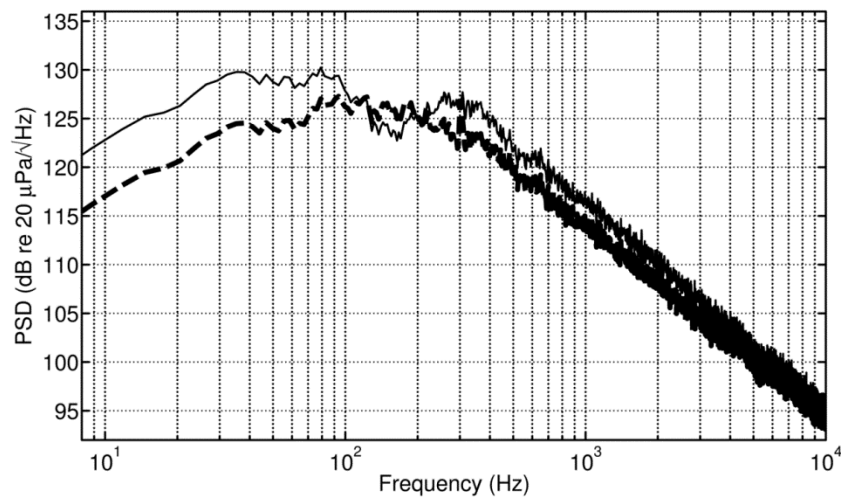


Figure 18. Measured and corrected PSDs using a 3.2 m microphone height, $\sigma_{eff} = 3000$ cgs rayls, $L = 2.5$ m, and $\langle \mu^2 \rangle = 1 \times 10^{-3}$.

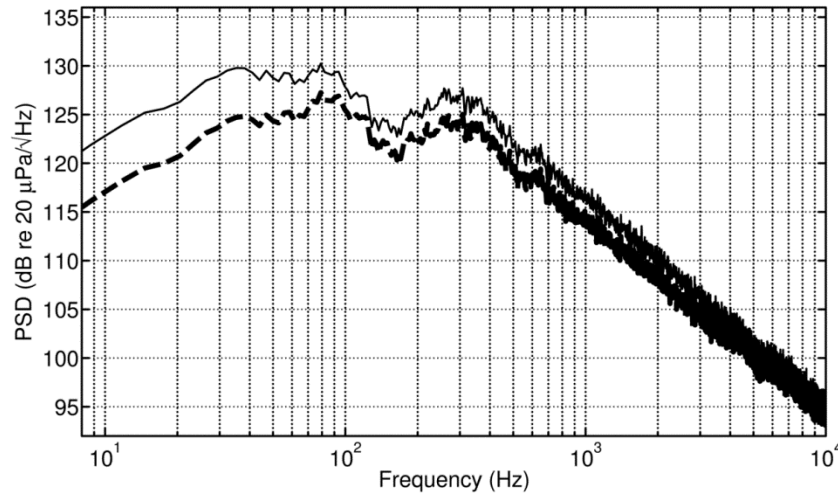


Figure 19. Measured and corrected PSDs using a 3.2 m microphone height, $\sigma_{eff} = 3000$ cgs rays, $L = 2.5$ m, and $\langle \mu^2 \rangle = 1 \times 10^{-2}$.

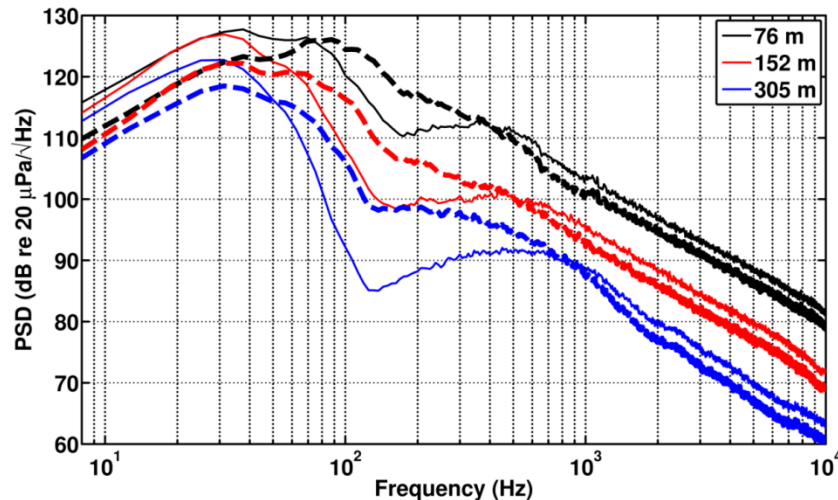


Figure 20. Figure 13, but with increased fluctuating index of refraction at 76 and 152 m: $\langle \mu^2 \rangle = 1 \times 10^{-4}$ at 76 m and $\langle \mu^2 \rangle = 5 \times 10^{-5}$ at 152 m. The 305 m index remains at $\langle \mu^2 \rangle = 1 \times 10^{-5}$.

4. Conclusion

The relative sound pressure level due to turbulent-atmosphere, finite-impedance ground reflections for extended distributions of correlated simple sources has been derived. The modeling has made it possible to apply corrections to measured rocket noise spectra. The fact that meaningful spectral corrections are obtained far from the plume using effective flow resistivities, turbulence length scales, and fluctuating indices of refraction based on values found in the literature inspires confidence in the plausibility of this modeling approach. However, the fact that improved near-plume spectral corrections were obtained by increasing the effective turbulence does not necessarily negate the physicality of the modeling approach; it may be, in fact, that the near-plume entrained flow and temperature fluctuations can be represented by much greater turbulence parameters.

In that vein, there is much to be done to further investigate nuances of the modeling, e.g., the assumptions and approximations that Daigle uses employs to derive and solve Eq. (1). We have identified cases for which the Daigle model returns a negative squared pressure, something not previously discussed in the literature, and we need to understand if this is a limit to the underlying theory or the approximations made in producing a solution. Furthermore, a more realistic source model could be used and a sensitivity analysis to the various input parameters performed. Finally, the entire process needs to be rigorously experimentally validated to ensure the spectral corrections that, at present, appear plausible, do, in fact, yield free-field spectra.

Acknowledgments

We are grateful for the support of Alexandria Salton of Blue Ridge Research and Consulting, LLC and NASA Marshall Space Flight Center, in particular R. Jeremy Kenny and Janice Houston. We are also indebted to Kevin Rees and Roy Norris at ATK Space Systems Test Services.

References

- (Daigle, 1978) G. A. Daigle, J. E. Piercy, and T. F. W. Embleton, "Effects of atmospheric turbulence on the interference of sound waves near a hard boundary," *J. Acoust. Soc. Am.* **64**, 622–630 (1978).
- (Daigle, 1979) G. A. Daigle, "Effects of atmospheric turbulence on the interference of sound waves above a finite impedance boundary," *J. Acoust. Soc. Am.* **65**, 45–49 (1979).
- (Daigle, 1983) G. A. Daigle, J. E. Piercy, and T. F. W. Embleton, "Line-of-sight propagation through atmospheric turbulence near the ground," *J. Acoust. Soc. Am.* **74**, 1505–1513 (1983).
- (Delany, 1970) M. E. Delany and E. N. Bazley, "Acoustical properties of fibrous absorbent materials," *Appl. Acoust.* **3**, 105–116 (1970).
- (Eldred, 1971) K.M. Eldred, "Acoustic Loads Generated by the Propulsion System", NASA SP-8072, (1971).
- (Embleton, 1983) T. F. W. Embleton, J. E. Piercy, and G. A. Daigle, "Effective flow resistivity of ground surfaces determined by acoustical measurements," *J. Acoust. Soc. Am.* **74**, 1239 – 1244 (1983).
- (Gee, 2009) K. L. Gee, J. H. Giraud, J. D. Blotter, and S. D. Sommerfeldt, "Energy-based acoustical measurements of rocket noise," AIAA paper 2009-3165, May 2009.
- (Giraud, 2010) J. H. Giraud, K. L. Gee, and J. E. Ellsworth, "Acoustic temperature measurement in a rocket noise field," *J. Acoust. Soc. Am.* **127**, EL179-EL184 (2010).
- (Johnson, 1987) M. A. Johnson, R. Raspet, and M. T. Bobak, "A turbulence model for sound propagation from an elevated source above level ground," *J. Acoust. Soc. Am.* **81**, 638–646 (1987).
- (Morgan, 2012) J. Morgan, T. B. Neilsen, K. L. Gee, A. T. Wall, and M. M. James, "Simple-source model of high-power jet aircraft noise," *Noise Control Eng. J.* **60**, 435–449 (2012).
- (Muhlestein, 2013) M. B. Muhlestein, K. L. Gee, T. B. Neilsen, and D. C. Thomas, "Prediction of nonlinear noise propagation from a solid rocket motor," *Proc. Mtgs. Acoust.* **18**, 040006 (2013).
- (Neilsen, 2013) T. B. Neilsen, K. L. Gee, A. T. Wall, and M. M. James, "Similarity spectra analysis of high-performance jet aircraft noise," *J. Acoust. Soc. Am.* **133**, 2116 – 2125 (2013).
- (Salomons, 2001) E. M. Salomons, V. E. Ostashev, S. F. Clifford, and R. J. Lataitis, "Sound propagation in a turbulent atmosphere near the ground: An approach based on the spectral representation of refractive-index fluctuations," *J. Acoust. Soc. Am.* **109**, 1881 – 1893 (2001).
- (Tam, 1995) C. K. W. Tam, "Supersonic jet noise," *Annu. Rev. Fluid Mech.* **27**, 17–43 (1995).